Sensitivity of Simulated Climate to latitudinal distribution of solar insolation reduction in Solar Radiation Management

Angshuman Modak* and Govindasamy Bala
Divecha Centre for Climate Change & Centre for Atmospheric and Oceanic Sciences
Indian Institute of Science
Bangalore – 560 012, India

*Corresponding author
Email: amatcaos@caos.iisc.ernet.in

Abstract

Solar radiation management (SRM) geoengineering has been proposed as a potential option to counteract climate change. We perform a set of idealized geoengineering simulations using NCAR CAM3.1 to understand the global hydrological implications of varying the latitudinal distribution of solar insolation reduction in SRM methods. To reduce the solar insolation we have prescribed sulfate aerosols in the stratosphere. The radiative forcing in the geoengineering simulations is the net forcing from a doubling of CO_2 and the prescribed stratospheric aerosols. We find that for a fixed total mass of sulfate aerosols (12.6 Mt of SO_4), relative to a uniform distribution which nearly offsets changes in global mean temperature from a doubling of CO_2, global mean radiative forcing is larger when aerosol concentration is maximum at the poles leading to a warmer global mean climate and consequently an intensified hydrological cycle. Opposite changes are simulated when aerosol concentration is maximized in the tropics. We obtain a range of 1K in global mean temperature and 3% in precipitation changes by varying the distribution pattern in our simulations: this range is about 50 % of the climate change from a doubling of CO_2. Hence, our study demonstrates that a range of global mean climate states, determined by the global mean radiative forcing, are possible for a fixed total amount of aerosols but with differing latitudinal distribution. However, it is important to note that this is an idealized study and thus not all important realistic climate processes are modeled.

(Key words: Climate Change, Geoengineering, Solar Radiation Management, Hydrological Cycle, Sulfate aerosols, Climate Model)

1. Introduction

Atmospheric concentrations of the greenhouse gases (GHGs) such as carbon dioxide (CO_2), methane (CH_4) and nitrous oxide (N_2O) have been increasing since pre-industrial periods primarily because of fossil fuel use and land-use change (IPCC, 2007). Their increase has the potential to cause long term climate change by altering the planetary radiation budget. To moderate future climate change and its impacts, several geoengineering proposals have been made recently. By definition, geoengineering is an intentional large-scale manipulation of the environment, particularly intended to counteract the undesired consequences of anthropogenic climate change (Keith, 2000).

Proposed geoengineering methods are classified into two main groups: Solar Radiation Management (SRM) methods and Carbon dioxide Removal (CDR) methods (Shepherd et al., 2009). In the first approach, the amount of solar absorption by the planet is reduced by artificially enhancing the planetary albedo so that the reduced insolation compensates the radiative forcing due to rising GHGs. Some proposed methods are injecting sulfate aerosols in the stratosphere (Budkyo,1982; Crutzen, 2006; Wigley, 2006) and placing space based sun shields in between the Sun and the Earth (Early, 1989). CDR methods propose to accelerate the removal of CO_2 from the atmosphere and thus they deal with the root cause of global warming (Shepherd et al., 2009).

Past climate modeling studies have modeled the effects of space-based SRM methods by reducing the solar constant (Govindasamy and Caldeira, 2000; Matthews and Caldeira, 2007; Caldeira and Wood, 2008; Lunt et al., 2008) or modeled the effects of stratospheric aerosol methods (Robock et al., 2008; Rasch et al., 2008a; Rasch et al., 2008b; Heckendorn et al., 2009; Jones et al., 2010). It has been shown (e.g., Bala et al., 2008) that SRM geoengineering would lead to a weakening of the global water cycle when the global mean temperature change is offset exactly. A recent study (Tilmes et al., 2013) using 12 models from Geoengineering Model Intercomparison Project (GeoMIP) confirms this weakening of hydrological cycle under multi-model framework. Further, it has been shown (Robock et al., 2008; Ricke et al., 2010; Tilmes et al., 2013) that the level of compensation will vary with residual changes larger in some regions than others. Therefore, some recent studies (Ban-Weiss and Caldeira, 2010; MacMartin et al., 2012) determine an optimal reduction in solar radiation in both space and time so the geoengineered world is more similar to the control climate while other studies (Irvine et al., 2010; Ricke et al., 2010) analyze the effect of different levels of uniform SRM forcing on regional climate response. Ban-Weiss and Caldeira (2010) vary both the amount and latitudinal distribution of aerosols to offset either the zonally averaged changes in surface temperature or the water budget. However, a simple and clear understanding of the effects of systematically varying the latitudinal distribution of aerosols and hence solar insolation reduction (e.g., more concentration in the tropics or high latitudes) on the hydrological cycle and surface temperature is lacking. In this study, we perform multiple idealized SRM geoengineering simulations with constant total amount of sulfate aerosols but with systematically varying latitudinal distribution.

We caution that our simulations are highly idealized and they are not meant to represent realistic latitudinal distribution of aerosols in geoengineering scenarios. Rather, they are designed to elucidate the fundamental properties of the climate system when the latitudinal distribution of aerosols and hence solar insolation reduction is systematically altered. We believe that our study should be considered as complementary to a previous work (Ban-Weiss and Caldeira, 2010), because not only we vary the latitudinal distribution of aerosols but we also provide a constraint by fixing the total amount of aerosols which facilitates a clear insight on the effects of varying the latitudinal distribution of aerosols.

2. Model and Experiments

We used the atmospheric general circulation model, CAM3.1 developed at the National Center for Atmospheric Research (NCAR) (Collins et al., 2004). It is coupled to the land model CLM3.0 and to a slab ocean model (SOM) with a thermodynamic sea ice model to represent the interactions with the ocean and sea ice components of the climate system. The model can be also configured with prescribed sea surface temperature and sea ice fraction. The horizontal resolution is 2° latitude and 2.5° longitude and the model has 26 vertical levels and the top of the model (TOM) is at 3hPa.

We performed two sets of simulations: 1) fixed-SST (sea surface temperature) simulations to estimate the radiative forcing which is measured as the net radiative flux change at the top of the atmosphere (Hansen et al., 1997). This method allows the rapid adjustment of the atmosphere and land components before radiative forcing is evaluated. The other set include the

SOM simulations to study the climate change. For both set of simulations, fixed-SST and SOM, we performed twelve cases: a control (1xCO_2),doubled CO_2 climate (2xCO_2) and ten geoengineering simulations each with differing latitudinal distribution of sulfate aerosol concentrations but with fixed total amount. The concentration of atmospheric CO_2 in 1xCO_2 is 390ppm and is 780ppm in 2xCO_2 and geoengineering simulations. The concentrations of other greenhouse gases are kept constant in all simulations. The background sulfate aerosol amount in this version of the model is 1.38 Mt SO_4. The fixed–SST simulations lasted for 30 years and the last 20 years are used to calculate the radiative forcing. The SOM simulations lasted for 60 years and the last 30 years are used for climate change analysis since all SOM simulations reach a near-equilibrium climate state in approximately 25 years.

As in Ban-Weiss and Caldeira (2010), the additional sulfate is prescribed in the geoengineering cases (Table 1, Figure 1a) and hence it is not transported around. However, in contrast to Ban-Weiss and Caldeira (2010), we introduce the constraint that the total amount of aerosol is constant (12.6 Mt SO_4) while latitudinal distributions are varied. Since aerosols are prescribed at TOM, the effect is essentially equivalent to making latitudinal changes to the solar constant. Sulfate aerosol particle size is prescribed and is assumed to be log-normally distributed with dry median radius ≈ 0.05μm and geometric standard deviation ≈ 2.0 (as used in a geoengineering scenario in a previous study (Rasch et al., 2008b)). The aerosol indirect effects are not modeled and aerosol loadings for other species like sea-salt, soil dust, black and organic carbon are unchanged in each of the simulations.

Besides a simulation with uniform aerosol concentration, our geoengineering simulations can be grouped into two categories: 1) Three "Tropics" simulations with maximum aerosol concentrations at the equator and 2) Six "Polar" cases with maximum concentrations at the poles. The latitudinal distribution of the stratospheric sulfate aerosol concentration are developed using the expression:

$$Q(\varphi) = a + b\cos(\varphi)$$

where Q is the concentration of the additional mass of sulfate aerosols, a and $b\cos(\varphi)$ are the uniform and non-uniform components of the distributions and φ represents the latitude. Both a and b are varied to obtain various distributions of concentrations (Table 1, Figure 1a). However, when Q is integrated over the sphere, the result is 12.6Mt in all the cases. Our choice of 12.6 Mt for Q is dictated by the uniform distribution case which had near-zero global mean temperature change relative to the control case. In each of the geoengineering simulations aerosol mass is added to the model background concentration at the TOM as was done in a recent study (Ban-Weiss and Caldeira, 2010). An experiment where the same total mass (12.6Mt) of aerosol is distributed uniformly over the globe between 61hPa to 9.8hPa (15 – 30km) with a maximum at 30hPa (22km) showed that the radiative forcing is nearly the same as in our uniform distribution geoengineering case and hence the main conclusions reached in this study are unlikely to be altered.

3. Results

3.1 Global mean Temperature and Precipitation Response

We find that the radiative forcing for doubling the atmospheric CO_2 ($2xCO_2$) to be 3.5 W/m^2 while the global mean surface temperature rise is about 2.1K and the precipitation increase is about 4.3% (i.e. ≈ 2%/K) in agreement with previous studies using the same model (Rasch et al., 2008b; Bala et al., 2009). The slopes in Figures 1c and 1d indicate a climate sensitivity of $0.53K/Wm^{-2}$ and precipitation sensitivity (% change in precipitation for unit change in radiative forcing) of $1.5\%/Wm^{-2}$ respectively, values that are similar to Bala et al. (2009).

The slight warming in the geoengineering case where forcing is close to zero (the case Polar 1 in Figure 1c) is because of the CO_2 physiological forcing (Betts et al., 2007; Cao et al., 2010) which is not counteracted by a decrease in solar flux. CO_2 physiological forcing refers to the direct physiological response of plants to elevated CO_2: the plant stomata open less widely and thus decrease the canopy transpiration which in turn reduces evapotranspiration and causes surface warming. Therefore, in the zero radiative forcing case where CO_2 radiative forcing is countered by the reduction in solar radiation, the CO_2-physiological forcing leads to a slight warming.

In agreement with past studies (e.g., Lunt et al., 2008; Bala et al., 2008; Tilmes et al. 2013), we find that in the geoengineering scenario with uniform distribution of aerosol there is a decline in precipitation though there is a near cancellation of surface temperature change (Figure 1b). This occurs because of differing fast response (changes that occur before global mean surface temperature) in precipitation for solar and CO_2-forcing (Allen and Ingram, 2002; Bala et al., 2008; Bala et al., 2009; Andrews et al., 2009): longwave absorption by CO_2 in the atmosphere can contribute to increased vertical stability and suppress precipitation but this fast response mechanism is nearly absent for solar forcing because the atmosphere is nearly transparent to solar radiation. However, since the slow response (changes that are associated with global mean surface temperature change) is same for CO_2 and solar forcings (Bala et al. 2010), the total changes in rainfall are larger to solar forcing than to equivalent CO_2 forcing. Because of this differing hydrological sensitivity to solar and CO_2 forcing, insolation reductions (in geoengineering scenarios) sufficient to offset the entirety of global-scale temperature increases would lead to a decrease in global mean precipitation. This suppression of precipitation is simulated in all geoengineering simulations (the regression line does not pass through the origin in Figure 1b).

Our geoengineering simulations with varying aerosol distributions indicate a linear relationship between the global mean surface temperature change and the precipitation change (Figure 1b). The regression lines do not pass through the origin which implies that none of the distribution can offset global mean temperature and precipitation simultaneously. Though the total amount of aerosols in each of the geoengineering simulation is fixed, we obtain a range of 1K (residual cooling of 0.3 K for the Tropics3 case to residual warming of 0.7 K for the Polar6 case) in global mean temperature and 3 % (residual drying of 2 % for Tropics3 case to residual increase of 1 % for the Polar6 case) in precipitation changes which are about 50 % or more of the changes that result from doubling of CO_2. This indicates that a range of climate states are possible for a constant amount of aerosols.

As the polar maximum of the aerosol concentration increases the global mean temperature increases with concomitant increase in global mean precipitation as implied by the linear relationship in Figure 1b. One of the polar maximum SRM simulations (Polar3) almost offsets the changes in global mean precipitation but it has a residual warming of 0.4°C. Our results are broadly in agreement with other modeling studies: in an Arctic geoengineering study (Caldeira and Wood, 2008) with reduced solar constant only over arctic, residual global mean warming and enhancements of global precipitation are found.

In contrast, as magnitude of the tropical maximum concentration increases both global mean temperature and precipitation decreases. One of the Tropics cases (Tropics1) where the temperature change is nearly zero shows a reduction in the global mean precipitation. The reduction in precipitation in our "Tropics" simulations are consistent with observed decline in precipitation over land, runoff and river discharge into the ocean following the tropical volcanic eruption Mount Pinatubo (15°N) in 1991 (Trenberth and Dai, 2007). Our "Tropics" simulations can be compared to Mount Pinatubo eruption because the distribution of aerosols in 'Tropics' simulations have reasonable resemblance to the distribution of volcanic aerosols after few weeks of the eruption (the volcanic aerosols occupied a latitude band of 20^{o} S to 30^{o} N (McCormick et al., 1995)). Interestingly, we find that in none of the geoengineering scenarios considered in this study, changes in global mean surface temperature and precipitation can be offset simultaneously over either land or ocean. We also notice that the hydrological sensitivity (% change in precipitation per unit change in temperature) is almost same over both land and ocean (Figure 1b). Here, we have defined the hydrological sensitivity over land (ocean) as the ratio of change in land (ocean) averaged precipitation to change in land (ocean) averaged surface temperature.

We find that the prescribed aerosols with different latitudinal distributions along with doubled CO_2 concentrations (geoengineering simulations) lead to different global mean forcings (Figure 1c and 1d). Since there are linear relationships between radiative forcing and the changes in global mean temperature (Figure 1c) and between temperature and precipitation changes (Figure 1b), we find a linear relationship between radiative forcing and precipitation changes (Figure 1d). The Polar geoengineering scenarios have positive residual radiative forcing while the Tropics scenarios have negative residual forcing because solar forcing is less effective over the poles relative to the tropics (Figure 1c). This is further confirmed in Figure 2 which shows that the Polar cases have smaller increase in planetary albedo compared to the Tropics cases. The radiative forcing associated with planetary albedo changes drive the temperature changes and thus the Polar cases have lower albedo changes relative to the uniform case and hence are warmer and wetter while opposite is true for Tropics cases.

The variation of global mean surface temperature and precipitation with global mean radiative forcing (Figure 1c and 1d) shows that as the maximum aerosol concentration over the poles increases (Polar1 to Polar6) the residual forcing increases and hence the global mean temperature and precipitation increase. Similarly, as the maximum aerosol concentration over the equator increases (Tropics1 to Tropics3), an opposite variation is noticed.

To further investigate the degree of departure of the different geoengineering simulations from the control, we calculate the root mean square difference between the *spatial patterns* in geoengineered climates and the control climate and normalize this root mean square difference by the standard deviation of the control scenario (NRMSD). A value less than 1 for NRMSD would suggest that the geoengineered climate is indistinguishable from the control climate. Further, the geoengineering simulation with the smallest value for this quantity is the one that is closest to the control. In our study, we find that the NRMSD for temperature increases as the maximum concentration of aerosols at the poles increases and the NRMSD for precipitation increases as tropical maximum is increased (Figure 3). When all grids in the latitude-longitude domain are considered the NRMSD (Figure 3a) shows large variations: 0.40 to 1.4 for surface temperature and 0.25 to 0.40 for precipitation. In case of NRMSD for zonal means (Figure 3b), the spread is relatively less: 0.30 to 0.95 for surface temperature and 0.27 to 0.38 for precipitation. The uniform case has the least distance from the origin in Figure 3, suggesting that it has the least NRMSD if the objective is to minimize root mean square difference in both temperature and precipitation simultaneously.

3.2 Precipitation and Temperature Response in Tropics and Poles

The change in zonal-mean surface temperature between the geoengineering cases and the control case (1xCO2) show, similar to changes in global annual mean values, a monotonic increase at each latitude with increased polar weighting (Figure 4a). We notice a similar monotonic increase in zonal-mean land and zonal-mean ocean surface temperature (Figures 5a and 5b). Further, we find that almost all geoengineering simulation show residual high latitude warming. In the Tropics cases, we find smaller residual warming in the high latitudes and cooler tropics. Similar to temperature changes, the change in zonal-mean precipitation between the geoengineering cases and the control case show a monotonic increase at each latitude with increased polar weighting (Figures 4b, 5c and 5d).We find large changes in precipitation in the tropics which is likely to be seen as shifts in the intertropical convergence zone (ITCZ) but closer examination (Figure 6) shows that the position of ITCZ remains the same in all the cases and the monotonic increase in precipitation with poleward weighting is clearly seen. The changes in zonal mean precipitation minus evaporation (water budget) are similar to changes in zonal mean precipitation (Figures 4c, 5e and 5f).

Figure 7 shows the spatial pattern of radiative forcing in selected simulations: 2xCO_2, Uniform, Polar3, Tropics1, Polar6 and Tropics3 cases. We notice that the radiative forcing in the

$2xCO_2$ case is significant over the whole globe but not significant in most regions in the geoengineering cases. The radiative forcing is positive in most locations in Polar cases. In the Tropics cases, the forcing is negative in the tropical regions and positive in polar regions.

In the $2xCO_2$ case, both temperature and precipitation changes are large and significant over the whole globe (Figure 8). The temperature increase over poles is much larger than in the tropics, in agreement with previous studies (Caldeira and Wood, 2008; Lunt et al., 2008; Matthews and Caldeira, 2007; Robock et al., 2008; Rasch et al., 2008b). The uniform geoengineering case (Uniform) shows mitigation in the temperature with reduced precipitation relative to $1xCO_2$. This is because of the different nature of the CO_2 forcing and solar forcing: solar forcing is larger in the tropics and smaller in the poles whereas the CO_2 forcing is uniform over the whole globe. In Polar3 case, the change in precipitation is largely offset but there is significant warming over large regions. However, temperature is largely offset in Tropics1 but there is decrease in precipitation relative to the uniform distribution case. The last four panels of Figure 8 shows the extreme cases; the case with largest polar weighting (Polar6) significantly warms the planet while the case with largest tropical weighting (Tropics3) overcools the planet with large reduction in precipitation.

4. Discussion and Conclusions

In this study, for a fixed total amount of sulfate aerosols which when distributed uniformly nearly offsets the global mean temperature change from a doubling of CO_2, there is a residual cooling when the aerosol concentration is maximized near the tropical regions and warming when concentration is maximized near the polar regions (Figure 1c). Consequent changes in global mean precipitation are simulated as dictated by the hydrological sensitivity of the model (Figure 1b). Our result that the global mean precipitation is reduced when aerosol concentration is maximized at the equator is in agreement with a recent study that shows a drastic reduction in tropical rainfall when aerosol concentration is maximum in the tropics (Ferraro et al. 2014). We also observe a similar monotonic increase in precipitation intensity as the maximum aerosol concentration over the poles increases (Figure 9, 10 and 11). The increases are of the order of 10% for low intensity (5^{th} percentile) and 2-3% for large intensity (99^{th} percentile) between the extreme cases (Tropics3 and Polar6). In order to confirm that global mean radiative forcing is sufficient to infer the global mean climate change we performed four additional geoengineering simulations with total amount of aerosols varied (10Mt, 11Mt, 13Mt, and 14Mt) for the uniform distribution case. We find that the global mean temperature and precipitation changes follow the changes in global mean forcing (Figure 12) for this set of simulations too.

In agreement with earlier studies (e.g., Bala et al., 2008), we find that both temperature and precipitation changes cannot be offset simultaneously. In agreement with this, not only in a simulation with uniform distribution but in all the geoengineering simulation with different latitudinal distribution (that is, even with non-uniform distribution of solar insolation reduction), we find that it is not possible to offset both temperature and precipitation changes simultaneously. The latitudinal distribution which offsets the warming leads to a drier climate while the distribution which offsets the precipitation results in a relatively warmer world (note that Bala et al. (2008) used a uniform solar insolation reduction). For a fixed total amount of aerosols but with different latitudinal distribution it is possible to achieve a range of global mean radiative forcing and thus a range of climate states.

Our findings should be viewed in the light of the limitations and uncertainties involved in this study. Our simulations are highly idealized as we have prescribed sulfate aerosol (to reduce the solar insolation) instead of injecting and transporting them. We have prescribed a fixed particle size distribution but particle size distribution would evolve with time and is shown to be important in precisely estimating the effects on different climate variables (Rasch et al., 2008b). Some modeling studies (Robock et al., 2008) have injected aerosol precursors into the stratosphere with fixed particle size distribution while other studies (Heckendorn et al., 2009; Pierce et al., 2010; Niemeier et al., 2010; Hommel and Graf, 2011; English et al., 2012) have demonstrated the importance of including the microphysics of particle growth. Further, we have focused our investigation primarily on global mean climate while several other studies (e.g., Robock et al., 2008; Irvine et al., 2010; Ricke et al., 2010) focused on regional disparities.

In this study, we have not considered the consequences of detailed stratospheric dynamics and sulfate aerosol chemistry on the ozone layer (Tilmes et al., 2009). Our model lacks a dynamic ocean and sea ice components, and thus the effects of deep ocean circulation are not modeled here. Further, in this model an interactive land carbon cycle is not included and hence the impact of changes in the diffuse fraction of surface solar radiation due to stratospheric aerosols could not be investigated. We intend to use a later version of the model that includes carbon cycle to investigate the impacts of altered diffuse radiation in a future study. However, we believe our results on temperature and precipitation is so fundamental that they would be unchanged when additional components and feedbacks are included.

In summary, for a fixed total mass of aerosols, we find that the global mean climate is warmer and wetter when aerosol concentration is maximum over the poles relative to the uniform distribution case (which offsets global mean temperature change) because the global mean residual radiative forcing is positive in these cases when compared to the uniform case. The opposite is true when aerosol concentration is maximum in the tropics. Further, our study clearly indicates that knowledge of global mean radiative forcing, not the details of latitudinal distribution of aerosols, is sufficient to infer the global mean climate change.

Acknowledgements. Financial support for A. Modak was provided by the Divecha Centre for Climate Change, Indian Institute of Science. We thank the Supercomputer Education and Research Centre, Indian Institute of Science for providing the computational resources.

References

1. Allen, M.R. and Ingram, W. J.: Constraints on future changes in climate and the hydrologic cycle, Nature, 419, 224-232, doi:10.1038/nature01092, 2002.
2. Andrews, T., Forster, P. M., and Gregory, J. M.:A surface energy perspective on climate change, J. Climate., 22, 2557-2570, doi: 10.1175/2008JCLI2759.1, 2009.
3. Bala, G., Caldeira K., and Nemani, R.: Fast versus slow response in climate change: implications for the global hydrological cycle, Clim. Dynam. 35, 423-434, doi: 10.1007/s00382-009-0583-y, 2009.
4. Bala, G., Duffy P. B., and Taylor, K. E.: Impact of geoengineering schemes on the global hydrological cycle, P. Natl. Acad. Sci. USA, 105, 7664-7669, doi:10.1073/pnas.0711648105, 2008.
5. Ban-Weiss, G. A. and Calderia, K.: Geoengineering as an Optimization Problem, Environ. Res. Lett., 5**,**034009, doi:10.1088/1748-9326/5/3/034009, 2010.
6. Betts, R. A., Boucher, O., Matthew, C., Cox, P. M., Falloon, P. D., Gedney, N., Hemming, D. L., Huntingford, C., Jones, C. D., Sexton, D. M. H., and Webb, M. J.: Projected increase in continental runoff due to plant responses to increasing carbon dioxide, Nature, 448, 1037–1041, doi:10.1038/nature06045, 2007.
7. Budkyo, M.I.: The Earth's Climate Past and Future, Academic, 1982.
8. Caldeira, K. and Wood, L.: Global and Arctic climate engineering: Numerical model studies, Philos. T. Roy. Soc. A, 366, 4039-4056, doi: 10.1098/rsta.2008.0132, 2008.

9. Cao, L., Bala, G., and Caldeira, K.: Climate response to changes in atmospheric carbon dioxide and solar irradiance on the time scale of days to weeks, Environ. Res. Lett.,7, 034015, doi:10.1088/1748-9326/7/3/034015, 2012.
10. Cao, L., Bala, G., Caldeira, K., Nemani, R., and Ban-Weiss, G. A.: Importance of carbon dioxide physiological forcing to future climate change, P. Natl. Acad. Sci. USA,doi:10.1073/pnas.0913000107, 2010.
11. Collins, W. D., Rasch, P. J., Boville, B. A., Hack, J. J., McCaa, J. R., Williamson, D. L., Kiehl, J. T., Briegleb, B., Bitz, C., Lin, S-J., Zhang, M., and Dai, Y.: Description of the NCAR community atmosphere model (CAM 3.0) NCAR Tech. Rep. NCAR/TN-464+STR National Center for Atmospheric Research Boulder CO 226pp, 2004.
12. Crutzen, P.J.: Albedo enhancement by stratospheric sulfur injections: A contribution to resolve a policy dilemma?, Climatic Change, 77, 211-220, doi: 10.1007/s10584-006-9101-y, 2006.
13. Early, J.T.: Space-based solar shield to offset greenhouse effect, Journal of the British Interplanetary Society, 42, 567-569, 1989.
14. English, J. M., Toon, O. B., and Mills, M. J.: Microphysical simulations of sulfur burdens from stratospheric sulfur geoengineering, Atmos. Chem. Phys.,12, 4775-4793, doi:10.5194/acp-12-4775-2012, 2012.
15. Ferraro, A. J., Highwood, E. J., and Charlton-Perez, A. J.: Weakened tropical circulation and reduced precipitation in response to geoengineering. Environ. Res. Lett., 9, 014001 doi: 10.1088/1748-9326/9/1/014001, 2014.
16. Govindasamy, B. and Caldeira, K.: Geoengineering Earth's radiation balance to mitigate CO_2-induced climate change, Geophys. Res. Lett., 27**,** 2141–2144, 2000.
17. Hansen, J., Sato, M., and Ruedy, R.: Radiative forcing and climate response J. Geophys. Res., 102(D6) 6831–6864, 1997.
18. Heckendorn, P., Weisenstein, D., Fueglistaler, S., Luo, B. P., Rozanov, E., Schraner, M., Thomason, L. W., and Peter, T.: The impact of geoengineering aerosols on stratospheric temperature and ozone, Environ. Res. Lett., 4**,** 045108, doi: 10.1088/1748-9326/4/4/045108, 2009.
19. Hommel, R. and Graf, H. F.: Modelling the size distribution of geoengineered stratospheric aerosols, Atmos. Sci. Lett., 12, 168-175, doi: 10.1002/asl.285, 2011.
20. Irvine, P. J., Ridgwell, A., and Lunt, D. J.: Assessing the regional disparities in geoengineering impacts, Geophys. Res. Lett., 37, L18702, doi: 10.1029/2010GL044447, 2010.
21. IPCC 2007 Climate Change 2007: The Physical Science Basis Contribution of Working Group 1 to the Fourth Assessment Report of the Intergovernmental Panel on Climate Change ed S Solomon, D Qin, M Manning, Z Chen, M Marquis, K B Averyt, M Tignor and H L Miller (Cambridge & New York: Cambridge University Press) 996 pp.
22. Jones, A., Haywood, J., Boucher, O., Kravitz, B., and Robock, A.: Geoengineering by stratospheric SO_2 injection: Results from the Met Office HadGEM2 climate model and comparison with the Goddard Institute for Space Studies ModelE, Atmos. Chem. Phys. Discuss., 10, 7421-7434, doi: 10.5194/acpd-10-7421-2010, 2010.
23. Keith, D. W.: Geoengineering the climate: history and prospect, Annu. Rev. Energ. Env., 25, 245–284, 2000.

24. Lunt, D. J., Ridgwell, A., Valdes, P. J., and Seale, A.: 'Sunshade world': a fully coupled GCM evaluation of the climatic impacts of geoengineering, Geophys. Res. Lett., 35**,** L12710, doi: 10.1029/2008GL033674, 2008.
25. Matthews, H. D. and Caldeira, K.: Transient climate-carbon simulations of planetary geoengineering, P. Natl Acad. Sci. USA, 104**,** 9949–9954, doi: 10.1073/pnas.0700419104, 2007.
26. MacMartin, D. G., Keith, D.W., Kravitz, B., and Caldeira, K.: Management of trade-offs in geoengineering through optimal choice of non-uniform radiative forcing, Nature Climate Change, doi: 10.1038/nclimate1722, 2012.
27. McCormick, M. P., Thomason, L. W., and Trepte, C. R.: Atmospheric effects of the Mt. Pinatubo eruption, Nature, 373, 399–404, 1995.
28. Niemeier, U., Schmidt, H., and Timmreck, C.: The dependency of geoengineered sulfate aerosol on the emission strategy, Atmos. Sci. Lett., 12**,**189-194, doi: 10.1002/asl.304, 2010.
29. Pierce, J. R., Weisenstein, D. K., Heckendorn, P., Peter, T., and Keith, D.W.: Efficient formation of stratospheric aerosol for climate engineering by emission of condensible vapor from aircraft, Geophys. Res. Lett., 37, L18805, doi: 10.1029/2010GL043975, 2010.
30. Rasch, P. J., Tilmes, S., Turco, R. P., Robock, A., Oman, L., Chen, C.C., Stenchikov, G.L., and Garcia, R. R.: An overview of geoengineering of climate using stratospheric sulphateaerosols, Philos. T. Roy. Soc. A, 366**,** 4007–4037, doi: 10.1098/rsta.2008.0131, 2008a.
31. Rasch, P. J., Crutzen, P. J., and Coleman, D. B.: Exploring the geoengineering of climate using stratospheric sulfate aerosols: The role of particle size, Geophys. Res. Lett., 35, L02809, doi: 10.1029/2007GL032179, 2008b.
32. Robock, A., Oman, L., and Stenchikov, G. L.: Regional climate responses to geoengineering with tropical and Arctic SO2 injections, J. Geophys. Res., 113, D16101, doi: 10.1029/2008JD010050, 2008.
33. Ricke, K. L., Morgan, M. G., and Allen, M. R.: Regional climate response to solar-radiation management, Nature Geosci., 3, 537 – 541, 2010.
34. Shepherd, J., Caldeira, K., Haigh, J., Keith, D., Launder, B., Mace, G., MacKerron, G., Pyle, J., Rayner, S., Redgwell, C., and Watson, A.: Geoengineering the climate: science, governance and uncertainty, The Royal Academy, 2009.
35. Tilmes, S., Garcia, R. R., Kinnison, D. E., Gettelman, A., and Rasch, P. J.: Impact of geoengineered aerosols on the troposphere and stratosphere, J. Geophys. Res., 114**,** D12305, doi: 10.1029/2008JD011420, 2009.
36. Tilmes et al.: The hydrological impact of geoengineering in the Geoengineering Model Intercomparison Project (GeoMIP). J. Geophys. Res. Atmos., 118, 11,036-11,058, doi: 10.1002/jgrd.50868, 2013.
37. Trenberth, K.E. and Dai, A.: Effects of Mount Pinatubo volcanic eruption on the hydrological cycle as an analog of geoengineering, Geophys. Res. Lett., 34, L15702, doi: 10.1029/2007GL030524, 2007.
38. Wigley, T. M. L.: A combined mitigation/geoengineering approach to climate stabilization, Science, 314, 452-454, doi: 10.1126/science.1131728, 2006.

Figure Captions

Figure 1: (a) Latitudinal profiles of sulfate aerosol concentration in the SRM geoengineering experiments. Polar1-6 have maximum concentration over the poles and Tropics1-3 have maximum at the equator. (b) Surface temperature change (K) vs precipitation change (%) relative to the 1xCO_2 case from slab ocean simulations (global mean values - squares, land mean values - stars, ocean mean values - triangles) . There is warming in all Polar cases relative to the uniform case and a concomitant increase in precipitation. Opposite is the case for Tropics cases. None of the regression lines pass through origin; temperature and precipitation cannot be offset simultaneously. In the case of land and ocean, ΔTS and ΔP represent the averages over the respective domain. (c) Radiative forcing (RF) vs surface temperature change. Polar cases have larger forcing relative to the uniform case and hence are warmer while opposite is true for Tropics cases. (d) Radiative forcing vs % precipitation change. Precipitation increases with residual RF (i.e. with increase in polar weighting) while decreases with increase in tropical weighting. In (b), (c) and (d) the horizontal and vertical bars represent the standard error of the respective variables which are calculated from the last 30 years of 60-year SOM simulations while in case of radiative forcing it is calculated from the last 20 years of 30-year fixed-SST simulations.

Figure 2: Change in planetary albedo in fixed-SST vs surface temperature change in slab ocean geoengineering simulations. The radiative forcing associated with albedo changes drive the temperature changes. Polar cases have lower albedo changes relative to the uniform case and hence are warmer and wetter while opposite is true for Tropics cases. The horizontal and vertical bars represent the standard error of the respective variables; temperature standard errors are calculated from the last 30 years of 60-year SOM simulations while albedo standard errors are calculated from the last 20 years of 30-year fixed-SST simulations.

Figure 3: Normalized root mean square difference (NRMSD) of surface temperature and precipitation between geoengineering and control simulation normalized by respective standard deviations computed for the global domain (top panel) and for the zonal averages (bottom panel).

The annual means of the last 30 years of the 60-year control simulation are used to estimate the standard deviation. Simulation nearest to x-axis represents the best precipitation mitigating scenario while the one closest to y-axis represents the best surface temperature mitigating scenario. Scenarios with maximum aerosol concentrations at the poles have larger NRMSD in temperature and conversely simulations with maximum at the equator have larger NRMSD in precipitation.

Figure 4: Zonal means of change in surface temperature (ΔTS), precipitation (ΔP) and precipitation minus evaporation (ΔPmE). (a) Zonal mean ΔTS increases monotonically with increase in maximum concentrations over the poles and decreases with increase in tropical maxima. (b) Zonal mean ΔP: polar maximum causes enhanced precipitation. (c) Zonal mean ΔPmE; polar maximum causes enhanced precipitation minus evaporation. Results shown are averages of the last 30 years of 60-year simulations.

Figure 5: Changes in zonal mean surface temperature (ΔTS), precipitation (ΔP) and precipitation minus evaporation (ΔPmE) over ocean (left panels) and land (right panels). (a) and (b): Zonal mean ΔTS increases monotonically with increase in the magnitude of maximum concentration of aerosols over poles and decreases with increase in the magnitude of tropical maximum. (c) and (d): polar maximum causes enhanced precipitation. (e) and (f): polar maximum causes enhanced precipitation minus evaporation. Results shown are averages of the last 30 years of 60-year simulations.

Figure 6: Zonal mean precipitation over the globe. The position of intertropical convergence zone (ITCZ) remains the same in all the geoengineering cases. The zonal mean precipitation decreases monotonically over the equator as the global mean radiative forcing increases. Results shown are averages of the last 30 years of 60-year simulations.

Figure 7: Spatial pattern of radiative forcing in the $2xCO_2$, uniform, and some Polar and Tropics geoengineering scenarios. In the Unifrom and Tropical cases, there is a residual positive forcing in the high latitudes and negative forcing in the low latitudes indicating an inexact compensation. Hatching indicates the region where the changes are significant at 1% level. Significance level

was estimated by Student's t test. Results shown are averages of the last 20 years of 30-year simulations with fixed sea surface temperature and sea ice fraction.

Figure 8: Changes in annual-mean surface temperature (left panels) and precipitation (right panels) in the $2xCO_2$, uniform, and some Polar and Tropics geoengineering scenarios relative to the control ($1xCO_2$). Hatching indicates the region where the changes are significant at 1% level. Significance level was estimated using Student's t-test. Both surface temperature and precipitation changes are large and significant everywhere in the $2xCO_2$ and extreme scenarios (Polar6 and Tropics3). Although significant over large regions, both temperature and precipitation changes are small in the Uniform case. Polar3 scenario offsets global mean precipitation but not global mean temperature while Tropics1 scenario offsets global mean temperature but with reduced precipitation. Results shown are averages of the last 30 years of 60-year simulations.

Figure 9: Percentile values (p5, p25, median, p75, p85, p90, p95 and p99)of precipitation intensity over Globe. There is a monotonic increase in precipitation for all percentile values as the maximum concentration of aerosols over poles increases. Grid-level monthly mean precipitation are used to calculate the percentile values.The last 30 years of 60-year simulations are used for the statistics.

Figure 10: Percentile values (p5, p25, median, p75, p85, p90, p95 and p99)of precipitation intensity over Land. There is a monotonic increase in precipitation for all percentile values as the maximum concentration of aerosols over poles increases. Grid-level monthly mean precipitation over all land points are used to calculate the percentile values.The last 30 years of 60-year simulations are used for the statistics.

Figure 11: Percentile values (p5, p25, median, p75, p85, p90, p95 and p99)of precipitation intensity over Ocean. There is a monotonic increase in precipitation for all percentile values as the maximum concentration of aerosols over poles increases. Grid-level monthly mean precipitation over all ocean points are used to calculate the percentile values.The last 30 years of 60-year simulations are used for the statistics.

Figure 12: (a) Radiative forcing (RF) vs surface temperature change. (b) Radiative forcing vs % precipitation change for uniform distribution scenarios with 10Mt, 11Mt, 12.6Mt, 13Mt and 14Mt. More aerosol mass leads to negative residual radiative forcing and hence cooler and drier climate, and smaller aerosol mass leads to positive residual radiative forcing and hence warmer and wetter climate. In (a) and (b) the horizontal and vertical bars represent the standard error of the respective variables. Results shown are averages of the last 20 years of 50-year SOM simulations for temperature and precipitation while the last 20 years of 40-year fixed-SST simulations are used for radiative forcing calculations.

Table 1: Description of different geoengineering experiments. Total additional mass is 12.6 Mt SO_4 in all the geoengineering simulations but the distribution varies.

Name of the Experiments	a (mg/m^2)	b (mg/m^2)	Total Mass from uniform component (Mt)	Total Mass from non-uniform component (Mt)	Total Mass (Mt)
Uniform	24.70	-	12.60	-	12.60
Polar1	23.52	3.19	12.00	0.60	12.60
Polar2	21.56	8.55	11.00	1.60	12.60
Polar3	19.60	13.89	10.00	2.60	12.60
Polar4	17.64	19.22	9.00	3.60	12.60
Polar5	15.68	24.56	8.00	4.60	12.60
Polar6	13.72	29.90	7.00	5.60	12.60
Tropics1	26.66	-5.34	13.60	-1.00	12.60
Tropics2	28.62	-10.67	14.60	-2.00	12.60
Tropics3	30.58	-16.02	15.60	-3.00	12.60

Figure 1

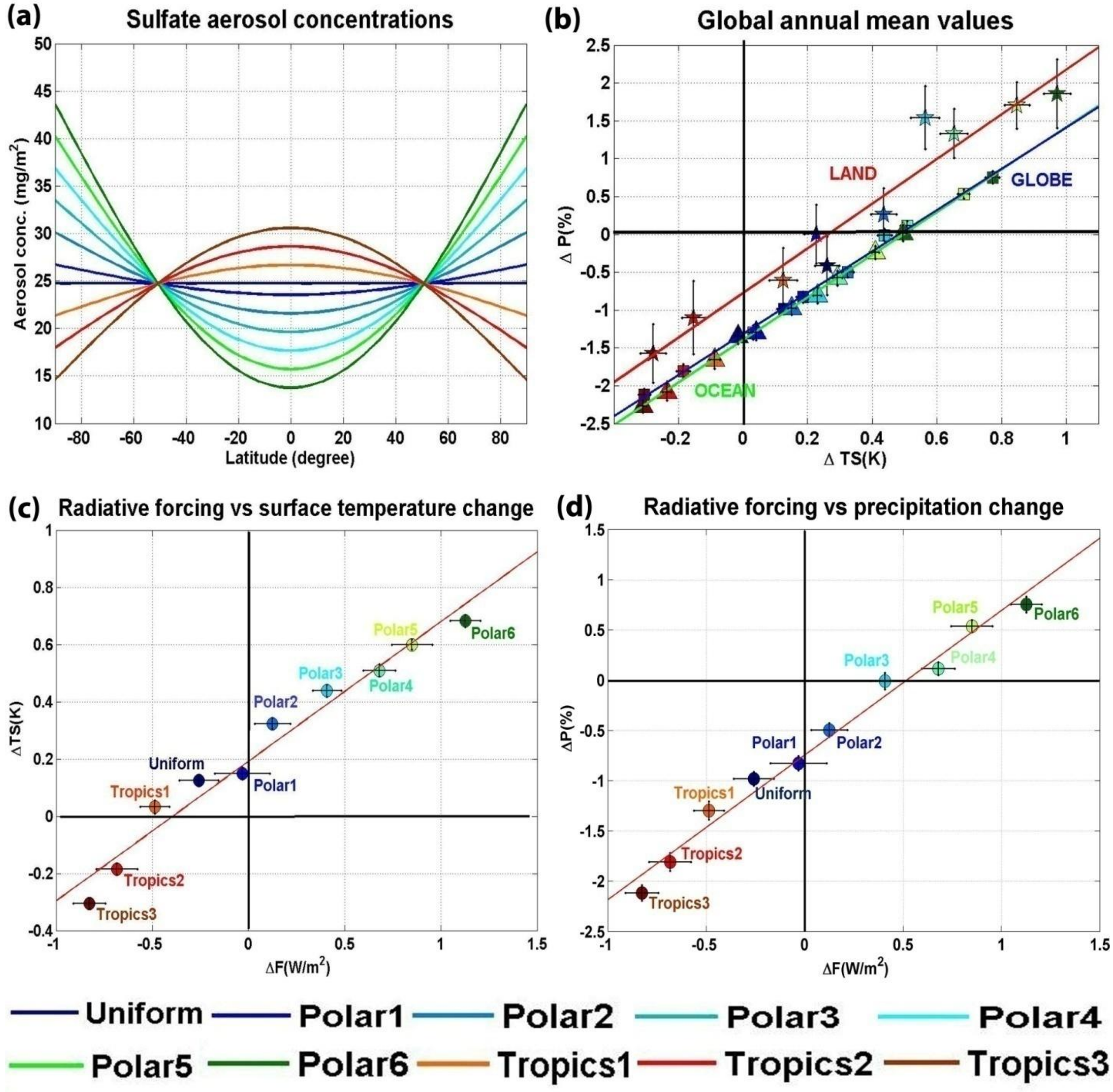

(a)
Sulfate aerosol concentrations
Aerosol conc. (mg/m²)
Latitude (degree)
(b)
Global annual mean values
LAND
GLOBE
OCEAN
Δ P(%)
Δ TS(K)
(c)
Radiative forcing vs surface temperature change
ΔTS(K)
ΔF(W/m²)
Uniform
Polar1
Polar2
Polar3
Polar4
Polar5
Polar6
Tropics1
Tropics2
Tropics3
(d)
Radiative forcing vs precipitation change
ΔP(%)
ΔF(W/m²)
Uniform
Polar1
Polar2
Polar3
Polar4
Polar5
Polar6
Tropics1
Tropics2
Tropics3
Uniform
Polar1
Polar2
Polar3
Polar4
Polar5
Polar6
Tropics1
Tropics2
Tropics3

Figure 2

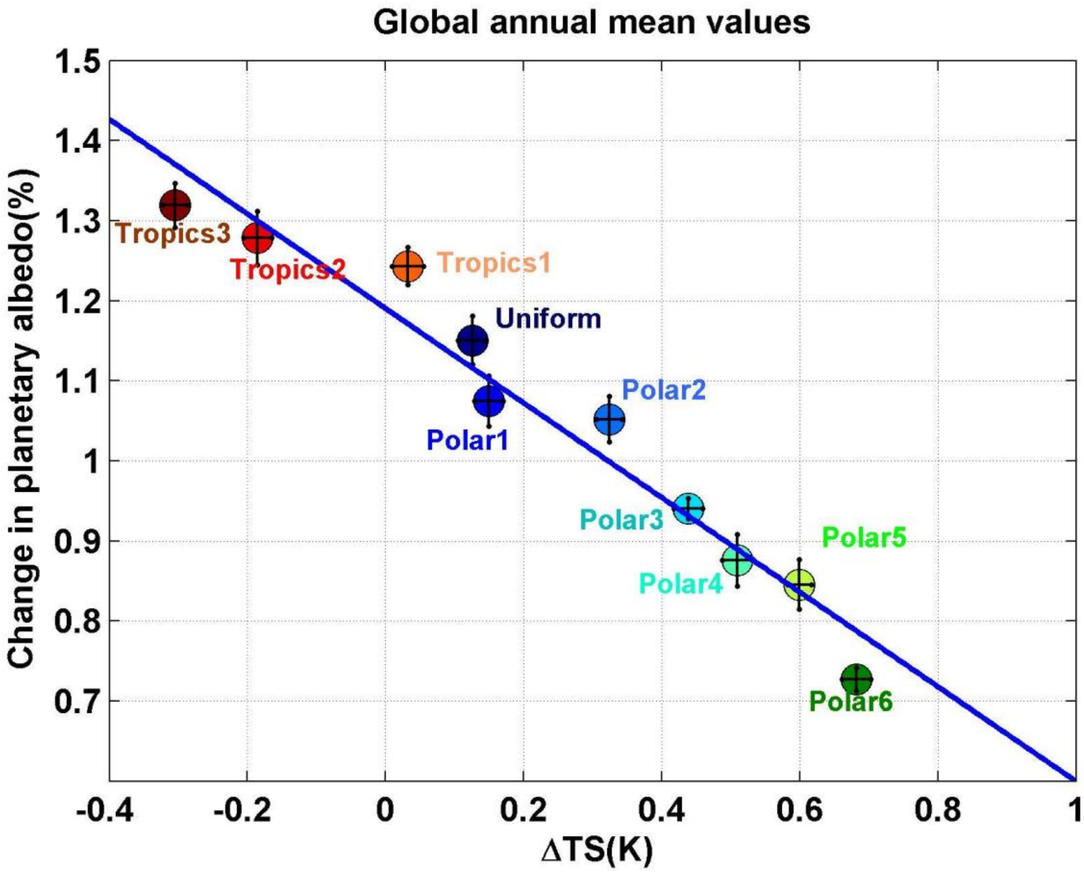
Global annual mean values
Change in planetary albedo(%)
ΔTS(K)
Tropics3
Tropics2
Tropics1
Uniform
Polar1
Polar2
Polar3
Polar4
Polar5
Polar6
1.5
1.4
1.3
1.2
1.1
1
0.9
0.8
0.7
-0.4
-0.2
0
0.2
0.4
0.6
0.8
1

Figure 3

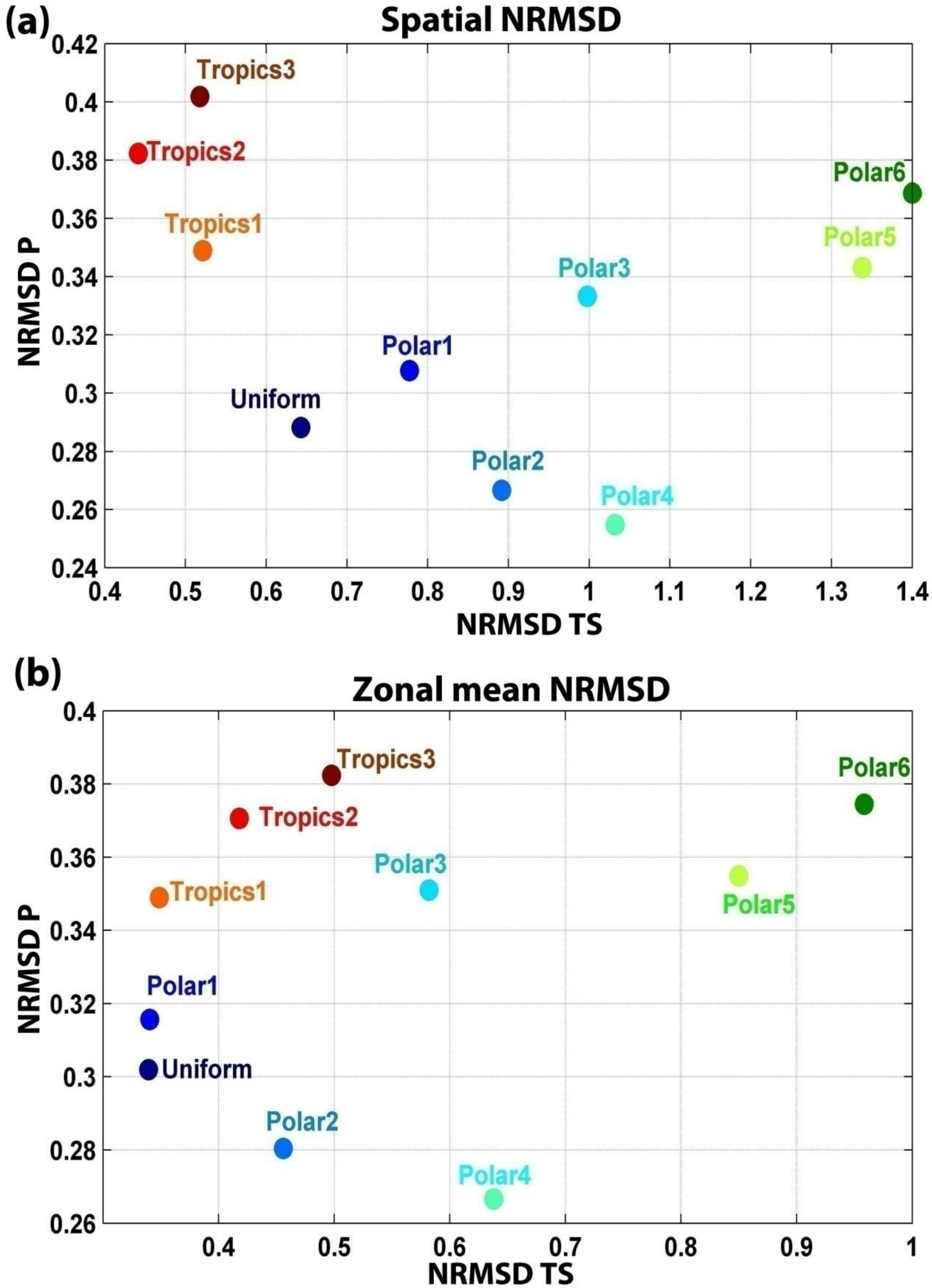
(a)
Spatial NRMSD
NRMSD P
NRMSD TS
0.42
0.4
0.38
0.36
0.34
0.32
0.3
0.28
0.26
0.24
0.4
0.5
0.6
0.7
0.8
0.9
1
1.1
1.2
1.3
1.4
Tropics3
Tropics2
Tropics1
Uniform
Polar1
Polar2
Polar3
Polar4
Polar5
Polar6
(b)
Zonal mean NRMSD
NRMSD P
NRMSD TS
0.4
0.38
0.36
0.34
0.32
0.3
0.28
0.26
0.4
0.5
0.6
0.7
0.8
0.9
1
Tropics3
Tropics2
Tropics1
Polar1
Uniform
Polar2
Polar3
Polar4
Polar5
Polar6

Figure 4

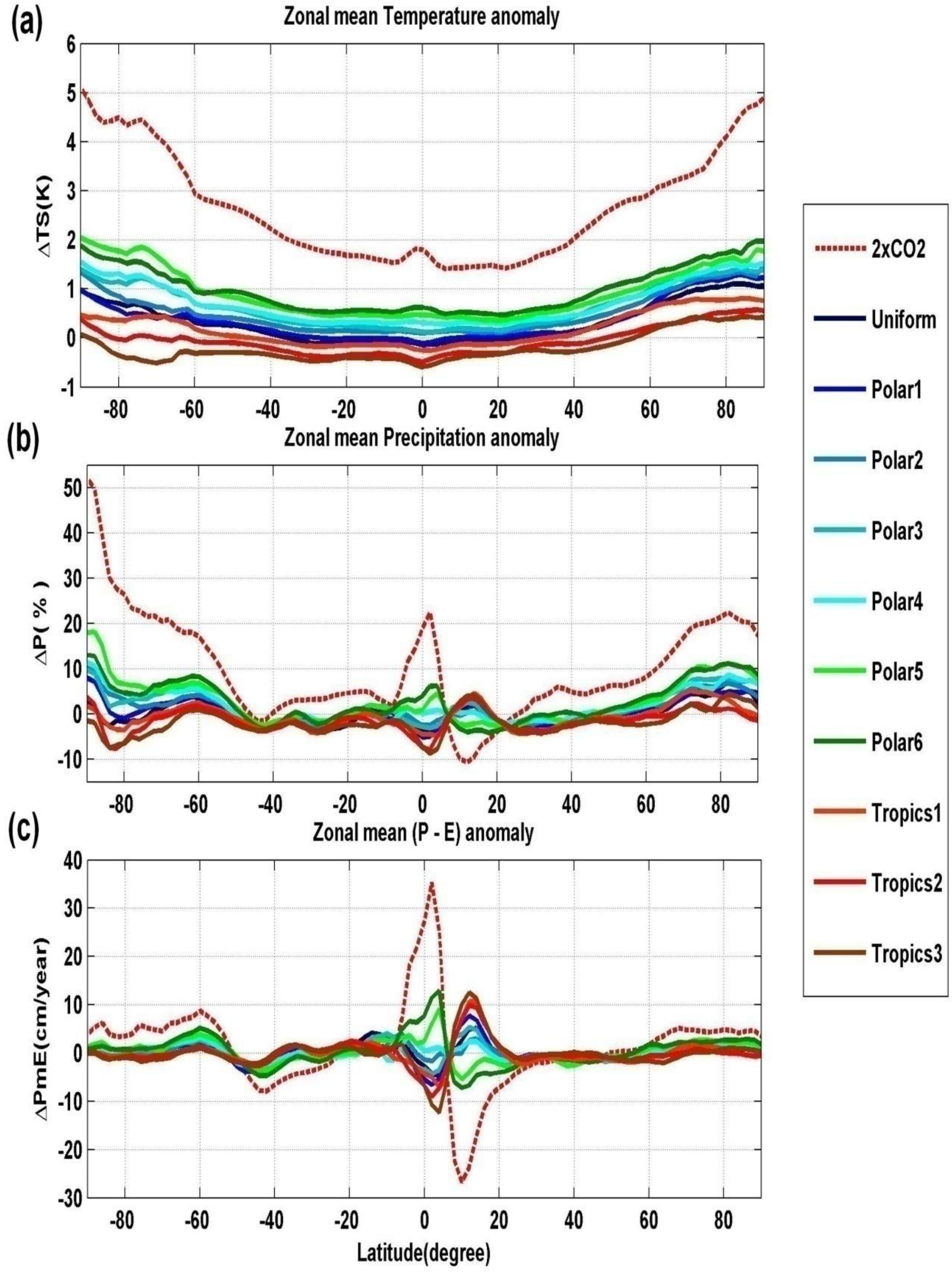
(a)
Zonal mean Temperature anomaly
ΔTS(K)
(b)
Zonal mean Precipitation anomaly
ΔP(%)
(c)
Zonal mean (P - E) anomaly
ΔPmE(cm/year)
Latitude(degree)
2xCO2
Uniform
Polar1
Polar2
Polar3
Polar4
Polar5
Polar6
Tropics1
Tropics2
Tropics3

Figure 5

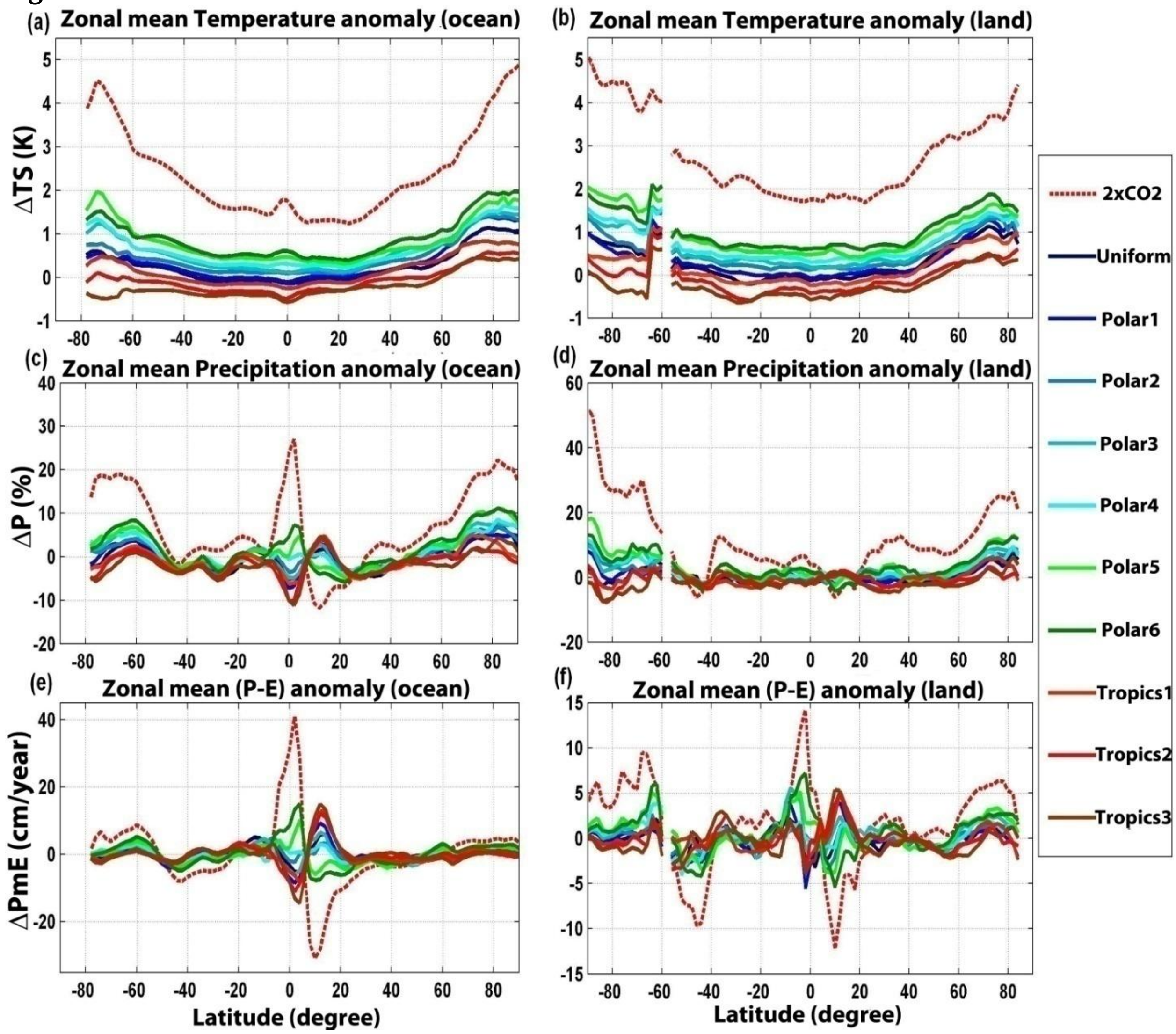
(a) Zonal mean Temperature anomaly (ocean)
(b) Zonal mean Temperature anomaly (land)
ΔTS (K)
(c) Zonal mean Precipitation anomaly (ocean)
(d) Zonal mean Precipitation anomaly (land)
ΔP (%)
(e) Zonal mean (P-E) anomaly (ocean)
(f) Zonal mean (P-E) anomaly (land)
ΔPmE (cm/year)
Latitude (degree)
Latitude (degree)
2xCO2
Uniform
Polar1
Polar2
Polar3
Polar4
Polar5
Polar6
Tropics1
Tropics2
Tropics3

Figure 6

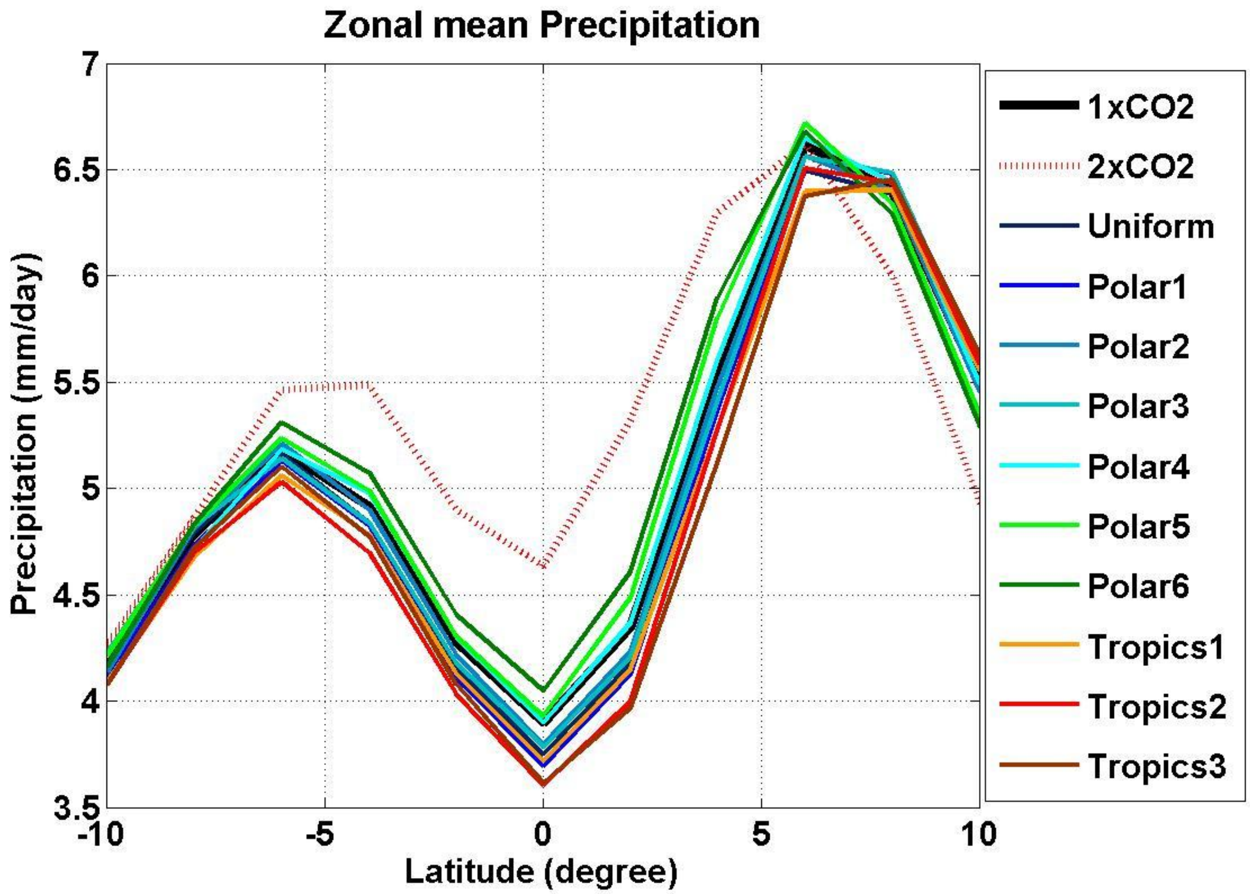
Zonal mean Precipitation
Precipitation (mm/day)
Latitude (degree)
7
6.5
6
5.5
5
4.5
4
3.5
-10
-5
0
5
10
1xCO2
2xCO2
Uniform
Polar1
Polar2
Polar3
Polar4
Polar5
Polar6
Tropics1
Tropics2
Tropics3

545 **Figure 7**

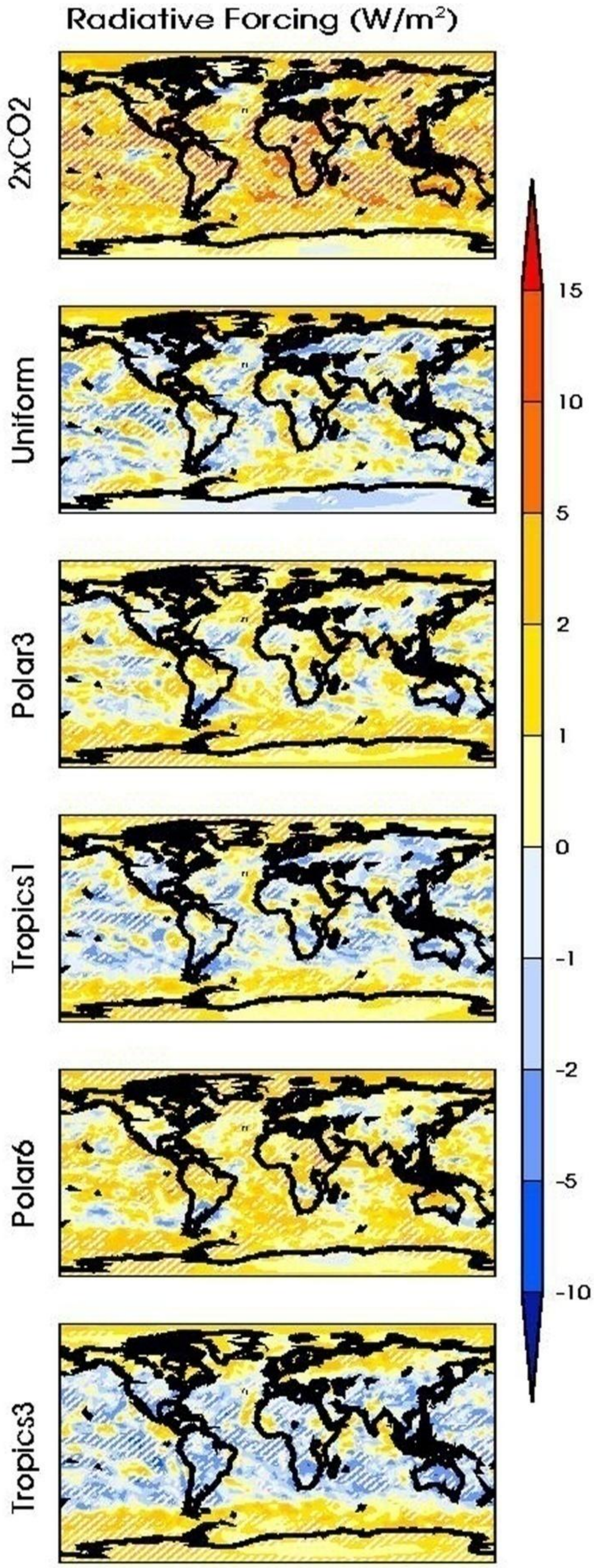

546

547 **Figure 8**

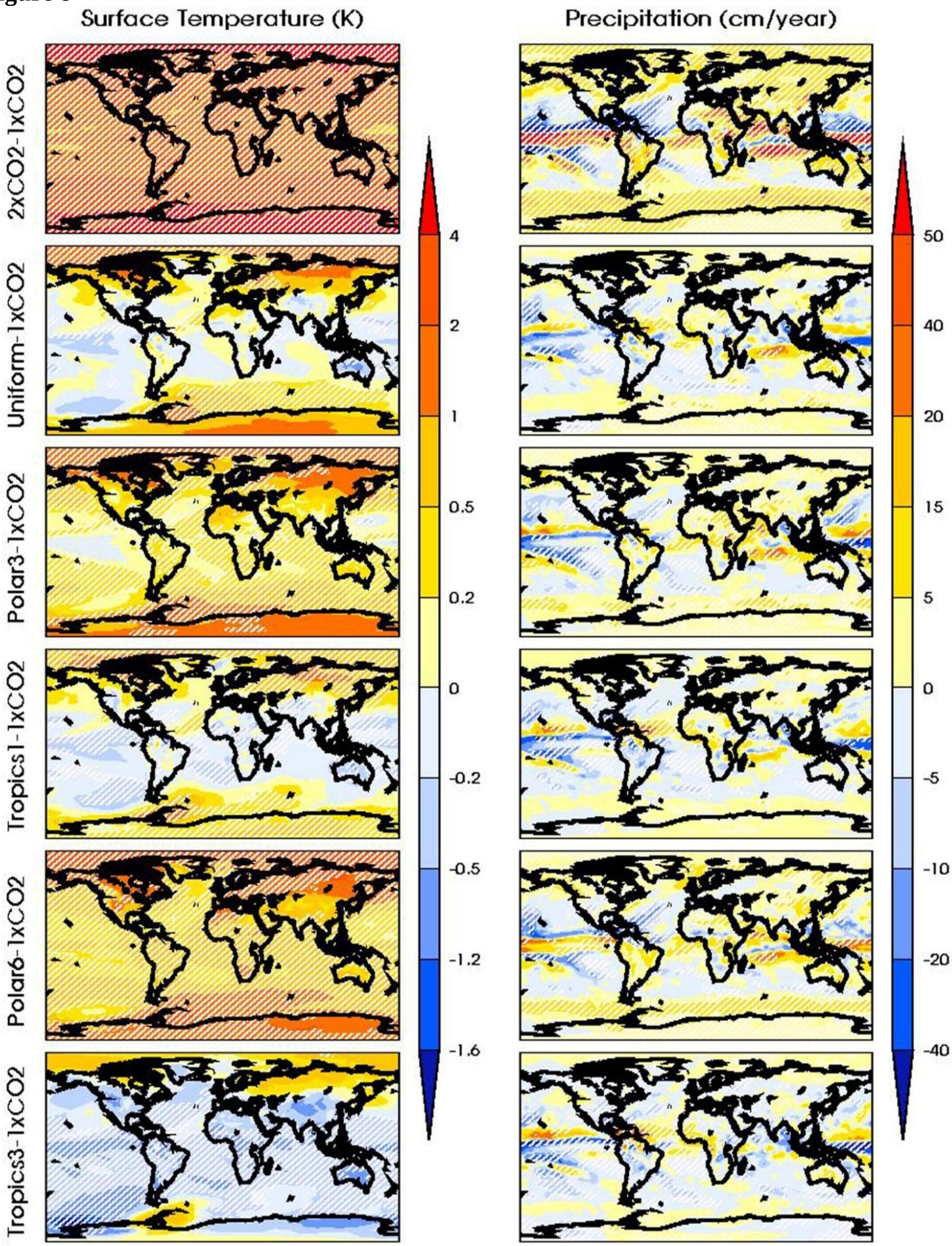

548
549

Figure 9

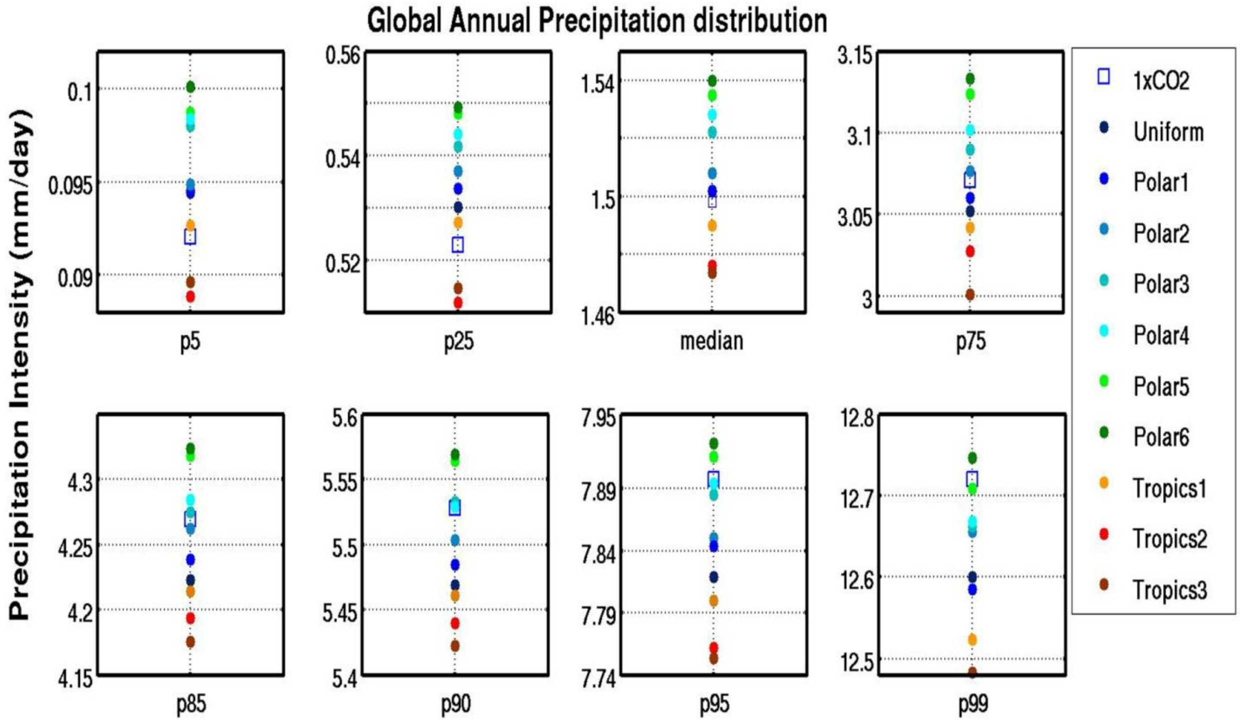

Global Annual Precipitation distribution
Precipitation Intensity (mm/day)
p5
p25
median
p75
p85
p90
p95
p99
1xCO2
Uniform
Polar1
Polar2
Polar3
Polar4
Polar5
Polar6
Tropics1
Tropics2
Tropics3

Figure 10

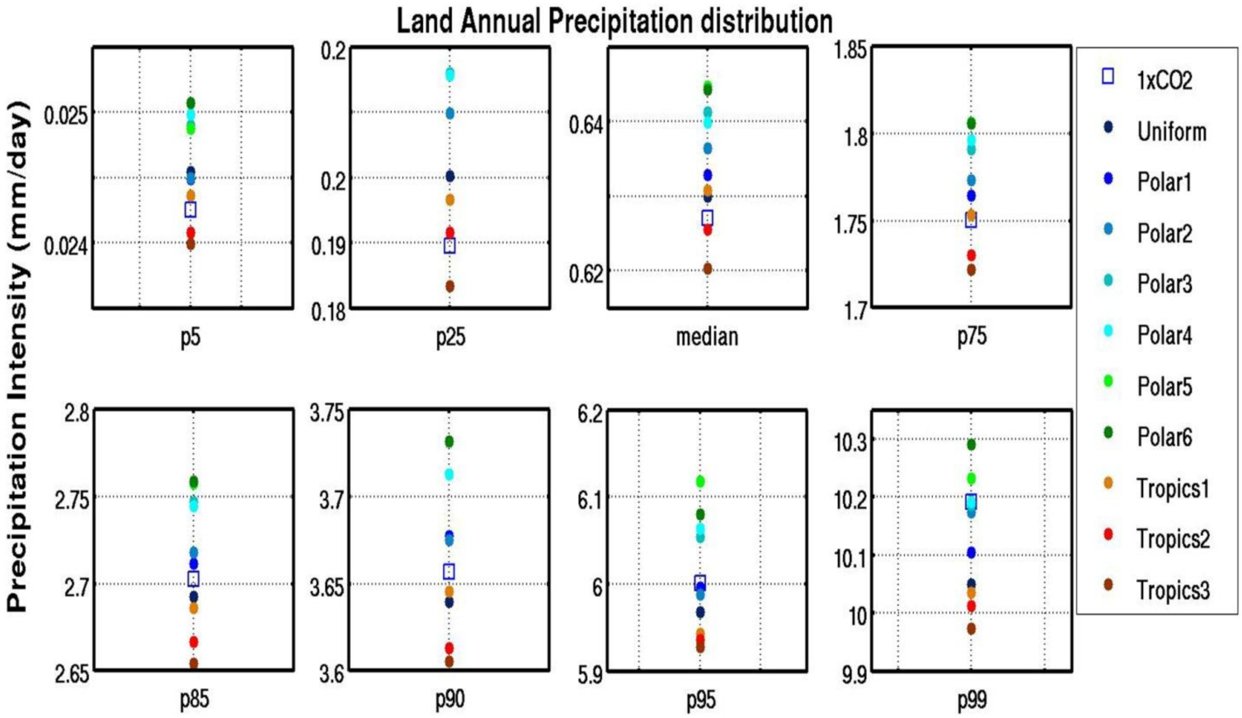
Land Annual Precipitation distribution
Precipitation Intensity (mm/day)
p5
p25
median
p75
p85
p90
p95
p99
1xCO2
Uniform
Polar1
Polar2
Polar3
Polar4
Polar5
Polar6
Tropics1
Tropics2
Tropics3

Figure 11

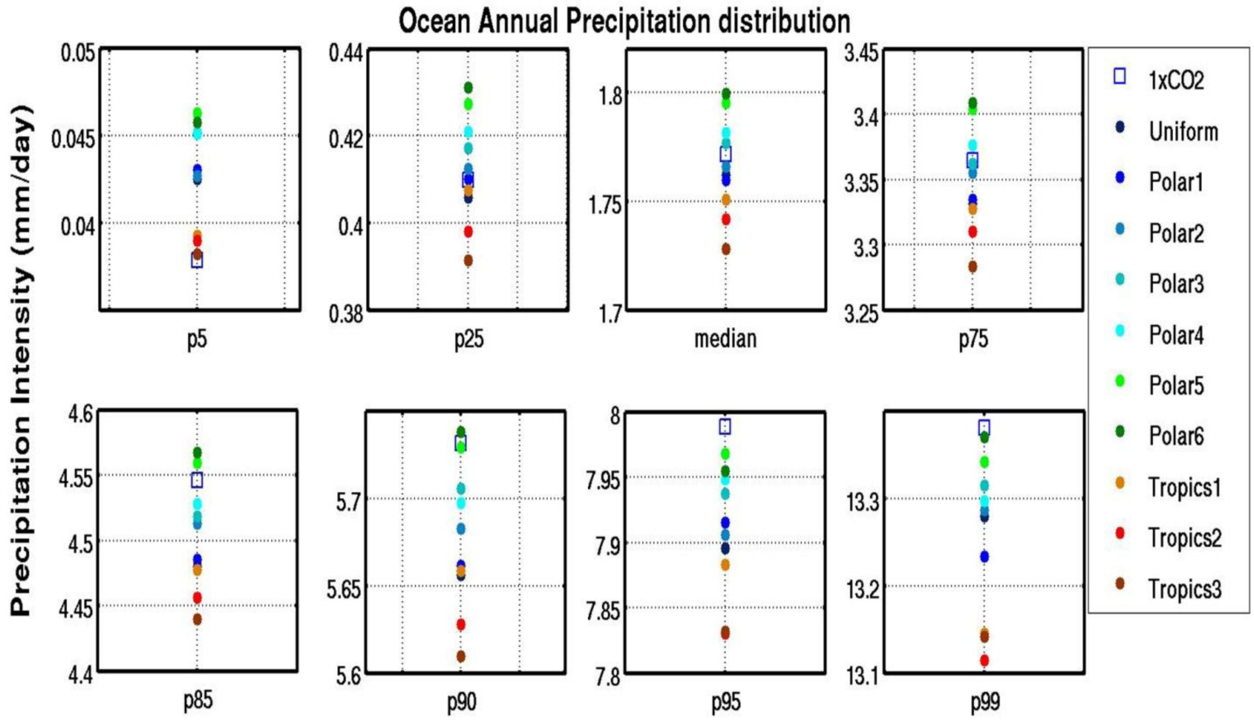
Ocean Annual Precipitation distribution
Precipitation Intensity (mm/day)
0.05
0.045
0.04
p5
0.44
0.42
0.4
0.38
p25
1.8
1.75
1.7
median
3.45
3.4
3.35
3.3
3.25
p75
4.6
4.55
4.5
4.45
4.4
p85
5.7
5.65
5.6
p90
8
7.95
7.9
7.85
7.8
p95
13.3
13.2
13.1
p99
1xCO2
Uniform
Polar1
Polar2
Polar3
Polar4
Polar5
Polar6
Tropics1
Tropics2
Tropics3

559 **Figure 12**

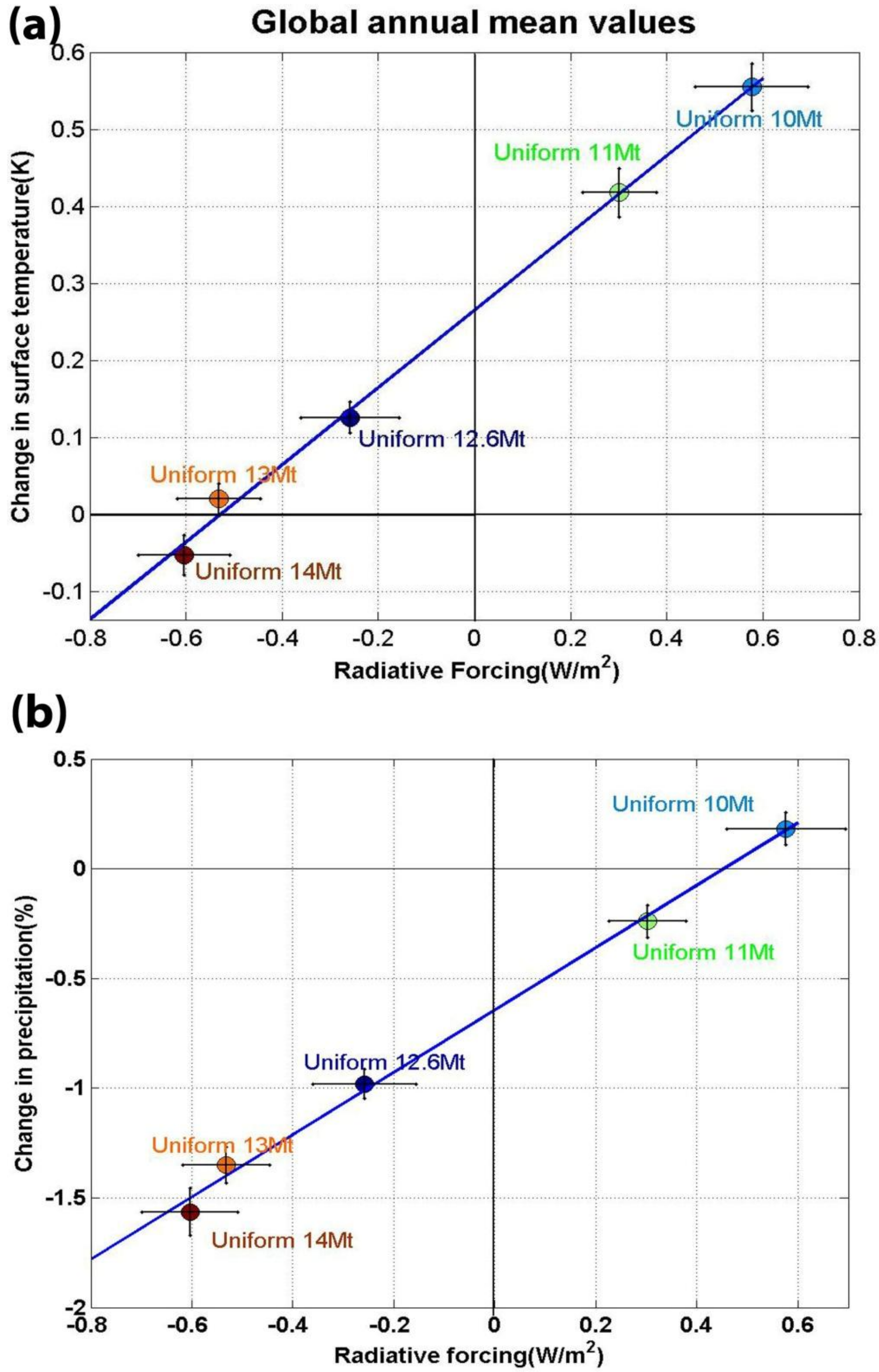

560